PHYSICAL REVIEW B **70**, 100101(R) (2004)

Probing cation antisite disorder in $Gd_2Ti_2O_7$ pyrochlore by site-specific near-edge x-ray-absorption fine structure and x-ray photoelectron spectroscopy

P. Nachimuthu,[1,2,*] S. Thevuthasan,[3] M. H. Engelhard,[3] W. J. Weber,[3] D. K. Shuh,[2] N. M. Hamdan,[2] B. S. Mun,[2] E. M. Adams,[3] D. E. McCready,[3] V. Shutthanandan,[3] D. W. Lindle,[1] G. Balakrishnan,[4] D. M. Paul,[4] E. M. Gullikson,[2] R. C. C. Perera,[2] J. Lian,[5] L. M. Wang,[5] and R. C. Ewing[5]

[1]*Department of Chemistry, University of Nevada, Las Vegas, Nevada 89154, USA*

[2]*Lawrence Berkeley National Laboratory, Berkeley, California 94720, USA*

[3]*Pacific Northwest National Laboratory, Richland, Washington 99352, USA*

[4]*Department of Physics, University of Warwick, Coventry, United Kingdom*

[5]*Department of Nuclear Engineering & Radiological Sciences, University of Michigan, Ann Arbor, Michigan 48109, USA*

(Received 7 May 2004; published 16 September 2004)

Disorder in $Gd_2Ti_2O_7$ is investigated by near-edge x-ray-absorption fine structure (NEXAFS) and x-ray photoelectron spectroscopy (XPS). NEXAFS shows Ti^{4+} ions occupy octahedral sites with a tetragonal distortion induced by vacant oxygen sites. O 1*s* XPS spectra obtained with a charge neutralization system from $Gd_2Ti_2O_7(100)$ and the $Gd_2Ti_2O_7$ pyrochlore used by Chen *et al.* [Phys. Rev. Lett. **88**, 105901 (2002)], both yielded a single peak, unlike the previous result on the latter that found two peaks. The current results give no evidence for an anisotropic distribution of Ti and O. The extra features reported in the aforementioned communication resulted from charging effects and incomplete surface cleaning. Thus, a result confirming the direct observation of simultaneous cation-anion antisite disordering and lending credence to the split vacancy model has been clarified.

DOI: 10.1103/PhysRevB.70.100101 PACS number(s): 66.30.Hs, 61.10.Ht, 72.80.Ng, 79.60.Ht

Pyrochlore materials are potentially useful for a range of technological applications.[1–4] In particular, their use in solid oxide fuel cells and as host matrices for actinide wastes are receiving increasing attention because of the recent discoveries showing that the isovalent substitution of Zr for Ti in $Gd_2Ti_2O_7$ results in a four to five orders-of-magnitude increase in the oxygen ion conductivity at 875 K and in resistance to energetic particle irradiation.[2,5] The mechanisms responsible for the large increase in these properties have been investigated by several experimental and theoretical methods.[3,4,6–10] These studies show that the increase in the ionic conductivity in pyrochlore is most likely due to the increased oxygen vacancies at the 48*f* site as a result of cation and anion disordering, which are responsible for the increased ionic conductivity.[3–5,8,9] The increased radiation tolerance is attributed to the ease of rearrangement and relaxation of Gd, Zr, and O ions/defects within the crystal structure, which inhibits amorphization by causing the irradiation-induced defects to relax and form cation antisite defects and anion Frenkel defects.[2] However, there is limited direct evidence for the presence of cation antisite disorder in a highly ordered pyrochlore structure.

Recently, Chen *et al.*[11,12] reported on the disorder in $Gd_2(Ti_{1-y}Zr_y)_2O_7$ pyrochlores measured by laboratory x-ray photoelectron spectroscopy (XPS), and the results provided direct evidence that cation antisite disorder occurs simultaneously with anion disorder. A key piece of information in these studies is the O 1*s* XPS spectra for $Gd_2Ti_2O_7$, which exhibits a broad feature with two components centered at binding energies (BEs) of ~526 and 531 eV. These component peaks were attributed to oxygen ions coordinated solely to Gd^{3+}, or to both Gd^{3+} and Ti^{4+} ions, respectively. The BE difference of ~5 eV between the two oxygen species is large for a single-phase compound. To obtain XPS spectra, Chen *et al.*[11,12] Ar^+-sputtered the surface, which removes contaminants but can preferentially deplete lighter elements from the surface region and induce defects/disorder. Although annealing under an oxygen partial pressure recovers the full oxygen stoichiometry and surface order in pyrochlore materials, the O 1*s* XPS feature has been shown to be insensitive to sputtering and subsequent annealing.[13]

In light of the XPS results from Refs. 11 and 12, the nature of disorder in $Gd_2Ti_2O_7$ pyrochlore has been reexamined using a multi-technique approach investigating the Ti 2*p* and O 1*s* of $Gd_2Ti_2O_7(100)$ by site-specific near-edge x-ray-absorption fine structure (NEXAFS) and XPS, as well as XPS of the same $Gd_2Ti_2O_7$ (and other pyrochlore compositions) employed in Refs. 11 and 12. NEXAFS involves electronic transitions originating from a selected atomic core level to unoccupied electronic states, which permits the determination of site-specific unoccupied electronic structure and site symmetry by use of linearly polarized x rays.[13] Laboratory XPS is used to provide information pertaining to the occupied electronic density of states from both pyrochlore materials that can be compared to the results from Refs. 11 and 12. The NEXAFS herein have about the same surface sensitivity as the XPS measurements.

Single crystals of $Gd_2Ti_2O_7$ were grown by the floating zone technique using an infrared image furnace.[14] The pyrochlore structure of the $Gd_2Ti_2O_7$ single crystal was confirmed by x-ray diffraction (XRD) and a series of pole figure measurements. Part of the crystal was powdered to measure the bulk lattice parameter ($a=1.01857$ nm) and confirmed the absence of secondary or minor phases.[14] The $Gd_2Ti_2O_7$ single crystal was cut and polished to obtain a (100) surface to better than 1°. The preparation and characterization of

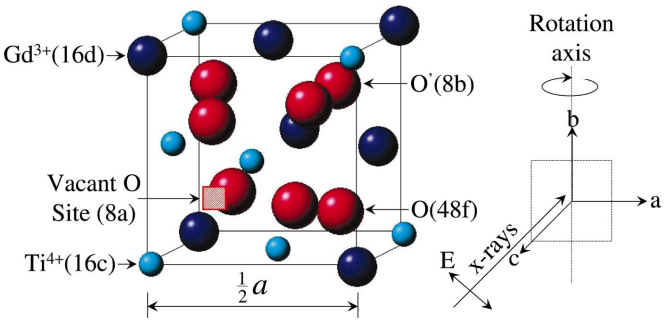

FIG. 1. (Color) Partial unit cell structure of $Gd_2Ti_2O_7$ pyrochlore. Gd^{3+} occupies the eight-coordinate A (16*d*) sites with six 48*f* and two 8*b* oxygen anions forming a distorted cube, whereas Ti^{4+} occupies six-coordinate B (16*c*) sites, which lie adjacent to the vacant 8*a* anion sites, forming a distorted octahedron with oxygen anions from 48*f* sites. Each oxygen anion in the 48*f* and 8*b* sites is tetrahedrally coordinated to two-of-each Gd^{3+} and Ti^{4+}, and four Gd^{3+} cations, respectively (Refs. 3, 7, and 10–12). The experimental geometry of $Gd_2Ti_2O_7(100)$ relative to the electric field vector (E) of the linearly polarized x rays is indicated (Ref. 16).

the $Gd_2Ti_2O_7$ pyrochlore used from Refs. 11 and 12 has been described.[11,12,15] Pyrochlores in general exhibit $A_2B_2O_6O'(Fd3m)$ stoichiometry and are a derivative of fluorite structure, but with two cations and one-eighth fewer anions. The unit cell contains 8 formula units and 4 nonequivalent sites. Fixing the origin at the B cation as in Fig. 1, the atoms A, B, O and O′ occupy $16d, 16c, 48f$, and $8b$ sites, respectively.[3,7,10–12]

Single crystals of $TiO_2(110), SrTiO_3(100)$, and Gd_2O_3 powder were utilized as NEXAFS references. Site-specific Ti 2*p* and O 1*s* NEXAFS were measured at Beamline 9.3.2 of the Advanced Light Source (ALS) at LBNL.[16] Figure 1 shows the experimental geometry relative to the electric field vector (E) of the x rays. Bulk-sensitive total fluorescence yield (TFY) NEXAFS signal was collected with a photodiode for several incidence angles. Spectra were corrected for the photon flux and then normalized to the edge jumps. The photon-energy was calibrated to the Ti $2p_{3/2}(t_{2g})$ absorption at 457.9 eV and O 1*s* pre-edge transition at 530.8 eV from $SrTiO_3(100)$. Resolution was 125 meV at 530 eV. XPS spectra were measured using a monochromatized Quantum 2000 spectrometer with a charge neutralization system. Clean and stoichiometric surfaces of $Gd_2Ti_2O_7(100)$ were prepared by 2 keV Ar^+-sputtering followed by annealing in 2×10^{-6} Torr of O_2 at 875 K. The $Gd_2Ti_2O_7$ pyrochlores from Refs. 11 and 12 were prepared in the same manner without the oxygen anneal.

The normal incidence ($\theta=0°$) NEXAFS spectra of $TiO_2(110)$ (rutile), $Gd_2Ti_2O_7(100), SrTiO_3(100)$, and Gd_2O_3 are shown in Fig. 2. The assignments of Ti 2*p* and O 1*s* NEXAFS features are made based on a symmetry-determined molecular orbital model obtained using the linear combination of atomic orbital method for the octahedral $(TiO_6)^{8-}$ ion cluster in TiO_2.[13] Spin-orbit interaction splits the Ti 2*p* into $2p_{3/2}(L_3)$ and $2p_{1/2}(L_2)$ states separated by ~5.4 eV. The $L_{3,2}$ transitions for $TiO_2, Gd_2Ti_2O_7$, and $SrTiO_3$ predominantly result from transitions to the final

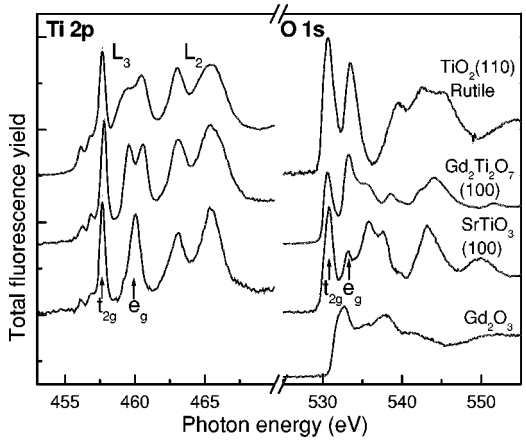

FIG. 2. Normal incidence ($\theta=0°$)Ti 2*p* and O 1*s* NEXAFS spectra from $TiO_2(110)$ (rutile), $Gd_2Ti_2O_7(100), SrTiO_3(100)$, and Gd_2O_3.

states, $(2p_{3/2,1/2})^{-1}d^1p^6$, where $(2p_{3/2,1/2})^{-1}$ denotes a hole in the $2p_{3/2}$ or $2p_{1/2}$ state. The t_{2g} and e_g result from transitions to the final states, $(2p_{3/2})^{-1}d(2t_{2g})^1p^6$ and $(2p_{3/2})^{-1}d(3e_g)^1p^6$, respectively. The energy separation between t_{2g} and e_g (crystal field splitting, 10 Dq) is ~2.2, ~2.3, and ~2.4 eV for $TiO_2, Gd_2Ti_2O_7$, and $SrTiO_3$, respectively. Comparison of Ti 2*p* NEXAFS from $Gd_2Ti_2O_7, TiO_2$, and $SrTiO_3$ shows that Ti is tetravalent and occupies sites of O_h symmetry in $Gd_2Ti_2O_7$. The e_g states, which consist of d_{z^2} and $d_{x^2-y^2}$ orbitals, are directed toward ligand anions and are sensitive to deviations from Ti O_h symmetry. Consequently, the splitting of e_g states into d_{z^2} and $d_{x^2-y^2}$ for $Gd_2Ti_2O_7$ is similar to TiO_2 and is dissimilar to $SrTiO_3$ in which Ti has perfect O_h site symmetry. This confirms that Ti occupies sites with distorted O_h symmetry in $Gd_2Ti_2O_7$. The energy separation between the d_{z^2} and $d_{x^2-y^2}$ orbitals of the e_g states is 1.0 and 1.2 eV for $Gd_2Ti_2O_7$ and TiO_2, respectively. This is a measure of the degree of distortion from pure O_h site symmetry and the Ti sites in $Gd_2Ti_2O_7$ are slightly less distorted than in TiO_2.

The O 1*s* transitions identified as t_{2g} and e_g in the NEXAFS spectra of Fig. 2 for $TiO_2, Gd_2Ti_2O_7$, and $SrTiO_3$ result from transitions to the final states, $3d(2t_{2g})^1(1s)^{-1}p^6$ and $3d(3e_g)^1(1s)^{-1}p^6$, respectively, where $(1s)^{-1}$ denotes a hole in the O 1*s* shell. The 10 Dq is 2.8, 2.7, and 2.5 eV for $TiO_2, Gd_2Ti_2O_7$, and $SrTiO_3$, respectively. The difference between the crystal field splitting observed in the Ti 2*p* and O 1*s* NEXAFS arises from the non-symmetric splitting of the e_g states into d_{z^2} and $d_{x^2-y^2}$ states which introduces complications in determining the 10 Dq from the Ti NEXAFS. This is substantiated by the close agreement of the 10 Dq observed in Ti 2*p* and O 1*s* NEXAFS for $SrTiO_3$ in which Ti^{4+} is in perfect O_h site symmetry. Comparison of the O 1*s* NEXAFS from $Gd_2Ti_2O_7$ to $TiO_2, SrTiO_3$, and Gd_2O_3 suggests that the oxygen ions coordinated to Gd^{3+} also contribute to the intensity in the vicinity of e_g states derived from the TiO_6 octahedron for $Gd_2Ti_2O_7$.

The normal incidence ($\theta=0°$) NEXAFS spectra of $Gd_2Ti_2O_7(100)$, where E of the x rays is parallel to the a axis ($E\|a$) are compared in Fig. 3 to the spectra measured at grazing incidence ($\theta=75°$) where E is nearly parallel to the

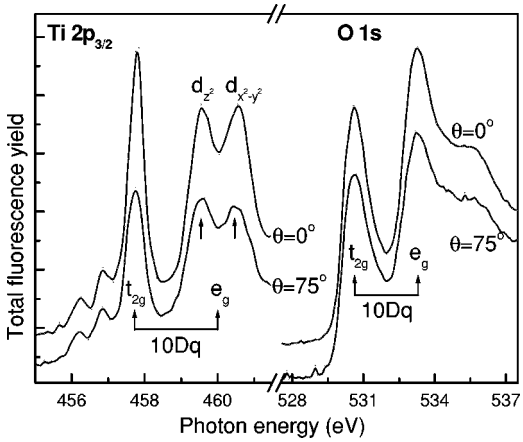

FIG. 3. Comparison of the normal ($\theta=0°$) to grazing incidence ($\theta=75°$)Ti $2p_{3/2}$ and O 1*s* NEXAFS from $Gd_2Ti_2O_7(100)$. The $\theta=0°$ polarization has the electric field vector (E) of the x rays parallel to the *a* axis ($E\|a$), whereas for $\theta=75°$, E is nearly parallel to the *c* axis ($E\|c$).

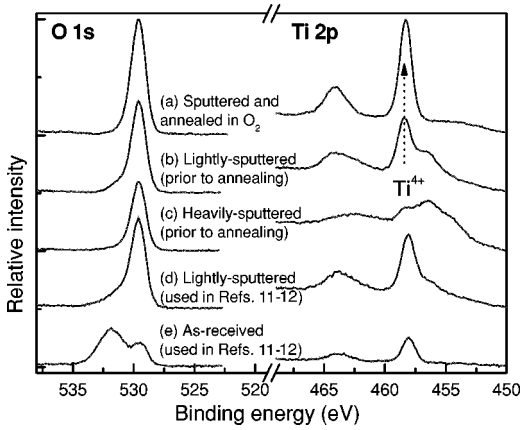

FIG. 4. Ti 2*p* and O 1*s* XPS spectra collected from $Gd_2Ti_2O_7(100)$ [spectra (a-c)] and the $Gd_2Ti_2O_7$ pyrochlore used in Refs. 11 and 12 [spectra (d-e)]. Spectra (a) was recorded after heavy Ar^+-sputtering followed by annealing under 2×10^{-6}Torr of O_2 at 875 K, whereas spectra (b-c) were recorded after light- and heavy-Ar^+-sputtering, respectively, prior to annealing in O_2. Spectra (d-e) were obtained from $Gd_2Ti_2O_7$ after light Ar^+-sputtering and as-received, respectively. The O 1*s* spectrum (d) was normalized to the intensity of the corresponding spectrum (b). This same normalization was employed for Ti spectrum (d). Spectra (e) were normalized using the same scaling factor relative to O 1*s* spectrum (d).

c axis ($E\|c$). The Ti 2*p* and O 1*s* NEXAFS measured at $\theta=0°$ and $\theta=75°$ predominantly probe unoccupied orbitals of Ti and O in $x(y)$ and *z* directions, respectively. No evidence for an anisotropic distribution of Ti and O sites was found. However, the intensities for the transitions to t_{2g} and e_g states in both Ti 2*p* and O 1*s* NEXAFS are significantly reduced for the $E\|c$ geometry compared to the $E\|a$. The intensity reduction for the transitions to t_{2g} states is also larger than for the e_g states in the Ti 2*p* NEXAFS. A similar intensity reduction is observed for the transition to the $d_{x^2-y^2}$ state relative to the d_{z^2} state within the e_g states. The decrease in spectral intensity for $E\|c$ compared to the $E\|a$ geometry reflects weaker covalence between Ti(d_{z^2}) and O(p_z) along the *c* axis with an elongated Ti-O distance providing additional support for a tetragonal distortion of the TiO_6 octahedron in $Gd_2Ti_2O_7$ as in TiO_2.[17] The e_g states, which are directly projected toward oxygen anions, split into lower energy d_{z^2} and higher energy $d_{x^2-y^2}$ states unlike the t_{2g} states. The vacant 8*a* oxygen sites located adjacent to the TiO_6 octahedron provide unoccupied density that also contributes to the intensities of the transitions to the t_{2g} and e_g states.[18] The large intensity for the transitions to t_{2g} and e_g states for $E\|a$ compared to the $E\|c$ geometry suggests vacant 8*a* oxygen sites are located in the *ab* plane adjacent to TiO_6 octahedra in $Gd_2Ti_2O_7$ which induces the tetragonal distortion.

Figure 4 shows the Ti 2*p* and O 1*s* XPS spectra recorded from $Gd_2Ti_2O_7(100)$ at different Ar^+-sputtering-times along with spectra after annealing under O_2, as well as the spectra from the corresponding $Gd_2Ti_2O_7$ material employed in Refs. 11 and 12 as-received and after light Ar^+ sputtering. The Ti XPS spectra from $Gd_2Ti_2O_7(100)$ show significant differences related to the duration of Ar^+-sputtering. The spectra before annealing show that Ti^{4+} is being reduced and give evidence for the preferential removal of oxygen from the surface. The spectrum after Ar^+-sputtering and annealing in 2×10^{-6} Torr of O_2 at 875 K, shows characteristics of Ti^{4+} indicating recovery of the fully stoichiometric surface. All of the O 1*s* XPS spectra collected [except for spectrum (e)] reveal a single peak at 529.6 eV with a full width at half maximum (FWHM) of ~1.5 eV regardless of Ar^+-sputtering time or if the pyrochlore has been annealed under O_2, although there is a slight decrease in spectral intensity before annealing. The O 1*s* spectrum (e) from the as-received $Gd_2Ti_2O_7$ sample shows the clear signature of C surface contamination at ~531 eV prior to sputtering. After light sputtering, the high BE component is almost fully removed, resulting in a single, narrow O 1*s* peak in spectrum (d). The observed O 1*s* feature at 529.6 eV for the $Gd_2Ti_2O_7$ materials is similar to that observed for TiO_2.[13] These results agree with previous XPS and NEXAFS studies of TiO_2 surfaces that indicate oxygen is preferentially sputtered while Ti at the surface is reduced.[13]

The results of this investigation, employing site-specific-NEXAFS and XPS to obtain corroborative information from two independent $Gd_2Ti_2O_7$ pyrochlores, including the same material used in the previous studies, contrast to the earlier results reported by Chen *et al.*[11,12] for $Gd_2Ti_2O_7$. The foremost difference between the results of the investigations is associated with the O 1*s* XPS spectra from the two pyrochlore materials examined in the current study that both yield a single, narrow peak at 529.6 eV with ~1.5 eV FWHM characteristic of Ti-O in $Gd_2Ti_2O_7$, whereas the previous study yielded broad O 1*s* features. The O 1*s* XPS spectra from the current study are also consistent with the corresponding NEXAFS spectra from $Gd_2Ti_2O_7(100)$. Thus, the O 1*s* XPS spectra reported by Chen *et al.*[11,12] consisting of a broad peak (>4 eV) composed of two components (~526 eV and 531 eV BE) assigned to oxygen ions coordinated solely to Gd^{3+} and to both Gd^{3+} and Ti^{4+} ions can be attributed to experimental complications difficult to discern when working with pyrochlores. The current results also ra-

tionalize why the components of the O 1*s* XPS features of Refs. 11 and 12 do not reflect the statistical distribution of oxygen sites as cross-sectional effects should be minimal and this is clearly not the case. Finally, the single peak found throughout in the current investigation reconciles the previously observed 5 eV O 1*s* chemical shift, which is somewhat large for similar metal-oxygen species in a single-phase material.

The discrepancies in the results between the current investigation and those from Chen *et al.*[11,12] clearly arise from complications due to the combination of surface charging effects and surface cleanliness during the previous XPS measurements. This has been confirmed by direct comparison of XPS spectra that were measured in the same spectrometer utilizing a charge neutralization system to negate charging effects and by careful observation of the surface contamination levels. The O 1*s* spectra in Refs. 11 and 12 exhibited peaks at BEs of ~526 and 531 eV that were shifted by charging and from surface hydrocarbon contamination, respectively. It is also interesting to note the surface preparation methodology used in the studies of Refs. 11 and 12 might be thought to have resulted in non-stoichiometric or disordered $Gd_2Ti_2O_7$ surfaces exhibiting broadened O 1*s* XPS features. However, based on knowledge from previous studies on pyrochlores[13] and the current work concerning the O 1*s* XPS spectra recorded after Ar^+-sputtering prior to annealing, the resultant O 1*s* core level feature should not be appreciable broadened (see Fig. 4). Lastly, the information provided by the NEXAFS spectra is in complete agreement with results of the XPS and the use of the TFY detection mode for the NEXAFS measurements completely avoids charging complications.

The site-specific NEXAFS show that Ti^{4+} ions in $Gd_2Ti_2O_7$ occupy sites of O_h symmetry with a tetragonal distortion, which is induced by the vacant 8*a* oxygen sites located in the *ab* plane adjacent to TiO_6 octahedra. Combined with the O 1*s* XPS spectra that show a single narrow peak characteristic of pristine Ti-O, as well as representative Ti 2*p* XPS spectra in both $Gd_2Ti_2O_7(100)$ and in the exact same $Gd_2Ti_2O_7$ pyrochlore used in Refs. 11 and 12, no evidence was found for an anisotropic distribution of Ti and O sites. The XPS and NEXAFS results are consistent for both Ti and O, and do not identify two distinct oxygen species corresponding to unique oxygen sites. The current results provide strong evidence that the observations of two different oxygen sites in $Gd_2Ti_2O_7$ by XPS with an O 1*s* BE difference of ~5 eV by Chen *et al.*[11,12] stem from experimental complications arising from sample charging and surface cleanliness. Therefore, the $Gd_2Ti_2O_7$ XPS results from Chen *et al.*[11,12] that provided direct evidence supporting the observation of simultaneous cation antisite disordering - anion disordering and lent partial support to the validity of the split vacancy model in pyrochlore materials have been clarified.

This work was supported by the Nevada DOE EPSCoR State-National Laboratory Partnership under Grant No. DE-FG02-01ER45898; U.S. Dept. of Energy (DOE) Offices of BES and BER and the EMSL User Facility at PNNL under Contract No. DE-AC06-76RLO-1830; DOE Office of BES, Divisions of Materials Sciences for ALS operations and Chemical Sciences, Geosciences, and Biosciences, both under Contract No. DE-AC03-76SF00098 at LBNL; an EPSRC grant at the University of Warwick, U.K.; the DOE Office of BES Grant No. FG02-97ER45656 at the University of Michigan.

*Corresponding author, Email address: PNachimuthu@lbl.gov

[1] R. C. Ewing, W. J. Weber, and J. Lian, J. Appl. Phys. **95**, 5949 (2004).
[2] W. J. Weber and R. C. Ewing, Science **289**, 2051 (2000).
[3] K. E. Sickafus, L. Minervini, R. W. Grimes, J. A. Valdez, M. Ishimaru, F. Li, K. J. McClellan, and T. Hartmann, Science **289**, 748 (2000), and references therein.
[4] J. A. Purton and N. L. Allan, J. Mater. Chem. **12**, 2923 (2002).
[5] H. L. Tuller, J. Electroceram. **1**, 211 (1997).
[6] C. Heremans, B. J. Wuensch, J. K. Stalick, and E. Prince, J. Solid State Chem. **117**, 108 (1995).
[7] N. J. Hess, B. D. Begg, S. D. Conradson, D. E. McCready, P. L. Gassman, and W. J. Weber, J. Phys. Chem. B **106**, 4663 (2002), and references therein.
[8] R. E. Willford and W. J. Weber, J. Am. Ceram. Soc. **82**, 3266 (1999); J. Nucl. Mater. **299**, 140 (2001).
[9] M. Pirzada, R. W. Grimes, L. Minervini, J. F. Maguire, and K. E. Sickafus, Solid State Ionics **140**, 201 (2001).
[10] J. Lian, X. T. Zu, K. V. G. Kutty, J. Chen, L. M. Wang, and R. C. Ewing, Phys. Rev. B **66**, 054108 (2002).
[11] J. Chen, J. Lian, L. M. Wang, R. C. Ewing, R. G. Wang, and W. Pan, Phys. Rev. Lett. **88**, 105901 (2002).
[12] J. Chen, J. Lian, L. M. Wang, R. C. Ewing, and L. A. Boatner, Appl. Phys. Lett. **79**, 1989 (2001).
[13] J. G. Chen, Surf. Sci. Rep. **30**, 1 (1997), and references therein.
[14] G. Balakrishnan, O. A. Petrenko, M. R. Lees, and D. M. Paul, J. Phys.: Condens. Matter **10**, L723 (1998).
[15] J. Lian, J. Chen, L. M. Wang, R. C. Ewing, J. M. Farmer, L. A. Boatner, and K. B. Helean, Phys. Rev. B **68**, 134107 (2003).
[16] Z. Hussain, W. R. A. Huff, S. A. Kellar, E. J. Moler, P. A. Heimann, W. McKinney, H. A. Padmore, C. S. Fadley, and D. A. Shirley, J. Electron Spectrosc. Relat. Phenom. **80**, 401 (1996).
[17] Z. Hu, M. Knupfer, M. Kielwein, U. K. Rößler, M. S. Golden, J. Fink, F. M. F. de Groot, T. Ito, K. Oka, and G. Kaindl, Eur. Phys. J. B **26**, 449 (2002).
[18] M. Merz, N. Nücker, P. Schweiss, S. Schuppler, C. T. Chen, V. Chakarian, J. Freeland, Y. U. Idzerda, M. Kläser, G. Müller-Vogt, and Th. Wolf, Phys. Rev. Lett. **80**, 5192 (1998).